Decoding the Stable Boundary Layer: Comparing Stable Conditions in the Arctic Stable Boundary Layer over Finland and Alaska

JORDAN ROBINSON*

National Weather Center REU
Norman, Oklahoma
Rhodes College
Memphis, Tennessee

BRIAN R. GREENE, FRANCESCA M. LAPPIN, AND ELIZABETH A. PILLAR-LITTLE
School of Meteorology and Center for Autonomous Sensing and Sampling
University of Oklahoma, Norman, OK

ABSTRACT

The boundary layer is one of the least understood areas of meteorology. The lowest kilometer of the troposphere, it is governed by the forces of the Earth's surface. At night, the boundary layer becomes negatively buoyant, creating a surface inversion layer. However, multiple layers of inversions are often present. In the arctic, stable conditions are nearly constant due to the presence of glaciers and sea ice. These conditions are particularly strong at night. Looking at profiles of the boundary layer from Northern Finland and North Alaska, temperature, potential temperature, wind, and relative humidity were examined in an effort to better understand conditions marking the stable boundary layer. Layered inversions were present over both locations, while Finland showed a more stable environment.

1. Introduction

Earth's atmosphere expands thousands of kilometers above its surface. The structure of the atmosphere is affected by pressure, gravity, and incoming radiation from the sun. However, the lowest kilometer of the atmosphere features an additional variable, the surface. Forcings-drag, friction, evaporation, transpiration, and terrain-alter the air immediately above the surface. Known as the atmospheric planetary boundary layer (PBL), this part of the atmosphere generally acts on timescales around a hour, with vertical and spatial scales of 1 km (Stull 2012). The convective boundary layer is characterized by a buoyant and turbulent atmospheric regime. Lapse rates decrease with height. Meaning, air parcels rise because the air above it is cooler. Turbulence is a function of the heating of the Earth's surface by the Sun's radiation. Surface heating of the lowest kilometer of the atmosphere and the transport of this heat in rising thermals leads to a regime characterized by entrainment and rapid mixing of air. However, this regime is reversed at night, (Stull 2012). As the downward transport of heat from the sun wanes, there is a net loss of heat from the surface through the atmosphere, or radiative cooling. As more heat escapes from the surface, the boundary layer becomes negatively buoyant, (Stull 2012). Turbulence is suppressed and little vertical movement of air occurs. These conditions are accelerated during the Arctic and Antarctic winter, where daylight lasts only a few hours. When conditions are sufficiently stable, these nocturnal transitions can be rapid (Mauritsen and Svensson 2007).

The boundary layer often exhibits a layered structure. These layers consist of inversions, where the lapse rates are positive, and stratified layers, where the magnitude changes but the sign of the lapse rate remains the same. In a study conducted by Mayfield and Fochesatto (2013), the occurrence of inversion layers is statistically quantified. Their study used radiosonde data from January 2000 to December 2009 taken from the National Oceanic and Atmospheric Administration (NOAA) Earth System Research Laboratory archive of radiosonde data from Fairbanks, Alaska International Airport (Mayfield and Fochesatto 2013). The total of 3633 radiosonde profiles included times 0000 and 1200 UTC. These profiles revealed a complex boundary layer structure composed of stratified, isothermal, and inversion layers. The inversion layers are an important aspect of the weather in Fairbanks. Situated in a valley, the entrapment of pollutants is an intermittent problem. Low level inversions prevent the rising

*Corresponding author address: Jordan Robinson, Rhodes College
2000 North Parkway Memphis, TN 38112
E-mail: jordanrobinson988@gmail.com

of air, including pollutants, into higher levels of the troposphere (Mayfield and Fochesatto 2013). In their paper, they develop a numerical procedure to analyze the depths, temperature, and dew point of the bottom and the top of the stratified/inversion layer and the embedded isothermal layers. Their algorithm was as follows,

$$\varepsilon = \|T(z) - \sum_k m_k z + b_k\|.$$

Here, T is the temperature profile, k is the number of profiles, m_k and b_k are function fitting parameters, and ε is the error function that was set at 1% error. The height of the top of an inversion layer was defined as the height above ground when the temperature gradient becomes negative as height increases. The top of a stratified level was defined as the height above ground where a change in the thermal gradient occurs, with the positive sign being maintained. They determined the mean height of the Surface Boundary Inversion (SBI) to be 377 m. The mean height of the first elevated inversion (EI-1) was determined to occur at 1231 m. The mean height of subsequent EI's occurred at 2125, 2720, and 3125 m, respectively (Mayfield and Fochesatto 2013).

The physics of the boundary layer is poorly understood. Observations collected in the boundary layer are sparse, even though meteorologists have numerous techniques of sampling the atmosphere. These include the use of remote sensing (Doppler radar, lidars and sodars), Automated Surface Observation Systems (ASOS), and radiosondes. These types of measurements fail to give us the whole picture. ASOS generally are only found in airports. Tools like radar are only found in select parts of the globe and have limited coverage and are not explicitly tuned to observe the thermodynamic properties of the atmosphere. Radiosondes are only released twice a day in select parts of the globe and spend minimal time in the PBL (Hoff and Hardesty 2012).

In studying the boundary layer, meteorologists make use of the Reynolds-Averaged Navier-Stokes Equations (RANS), which generally takes the following X-component form:

$$\begin{aligned}\frac{\partial \bar{u}}{\partial t} + \bar{u}\frac{\partial \bar{u}}{\partial x} + \bar{v}\frac{\partial \bar{u}}{\partial y} + \bar{w}\frac{\partial \bar{u}}{\partial z} \\ = \frac{-1}{\rho}\frac{\partial \bar{p}}{\partial x} + f\bar{v} - \frac{\partial \overline{u'u'}}{\partial x} - \frac{\partial \overline{v'u'}}{\partial y} - \frac{\partial \overline{w'u'}}{\partial z} \\ + \nu\left(\frac{\partial^2 \bar{u}}{\partial x^2} + \frac{\partial^2 \bar{u}}{\partial y^2} + \frac{\partial^2 \bar{u}}{\partial z^2}\right) \quad (1)\end{aligned}$$

The components of this equation generally represent the following:

1. $\frac{\partial \bar{u}}{\partial t}$: Local time rate of change of the mean u wind
2. $\bar{u}\frac{\partial \bar{u}}{\partial x}$: Advection of the mean u wind by the mean u wind.
3. $\bar{v}\frac{\partial \bar{u}}{\partial y}$: Advection of the mean u wind by the mean v wind
4. $\bar{w}\frac{\partial \bar{u}}{\partial z}$: Advection of the mean u wind by the mean w wind
5. $\frac{-1}{\rho}\frac{\partial \bar{p}}{\partial x}$: Pressure gradient force induced by the mean pressure field
6. $-\frac{\partial \overline{u'u'}}{\partial x} - \frac{\partial \overline{v'u'}}{\partial y} - \frac{\partial \overline{w'u'}}{\partial z}$: Divergence of the x-component of the turbulent kinematic momentum fluxes
7. $\nu(\frac{\partial^2 \bar{u}}{\partial x^2} + \frac{\partial^2 \bar{u}}{\partial y^2} + \frac{\partial^2 \bar{u}}{\partial z^2})$: Viscous dissipation of momentum

The x-component of this equation alone leave us with many, often instantaneous terms. These terms are nearly impossible to directly measure even with today's technology. Therefore, it is extremely difficult to analyze boundary layer conditions using the RANS with the limited data we do have. This lack of data is referred to as the PBL gap (Hoff and Hardesty 2012; National Research Council 2007; National Academies of Sciences 2018b,a). This gap is much more immense in relation to stable boundary layer conditions. Our poor understanding of the stable boundary layer translates into our weather models (Steeneveld et al. 2008). Numerical and climatic models have shown significant sensitivity to model mixing formulations in stable conditions (Holtslag et al. 2013). Additionally, the weak and intermittent turbulence found in stable conditions are difficult for models to resolve (Mauritsen and Svensson 2007; Sun et al. 2015; Sandu et al. 2013; Andreas et al. 2010; Kaiser et al. 2020). Several studies have focused on examining turbulence in the stable boundary layer using large eddy simulations (e.g., Beare et al. 2006; Sullivan et al. 2016; Couvreux et al. 2020), which have the advantage of explicitly resolving turbulence. However, the grid spacing requirements in these experiments are not realistic for operational forecasting models. Ideally, better observations of the PBL can enhance the collective understanding of stable boundary layer physics, which in turn can improve these operational models. Since stable conditions are near constant in the arctic, it is an ideal place to gather data in an aim to fill in this gap.

Using data taken from two opposite ends of the Arctic, this study will examine the presence of a layered structure in the stable boundary layer as well as compare and analyze various atmospheric state variables. Specifically, profiles of temperature, potential temperature, moisture, and wind will be evaluated. In addition, the presence of multiple layers of inversions will be examined.

2. Methods

My analysis utilizes data taken during the 2018 Innovative Strategies for Observations in the Arctic Atmospheric

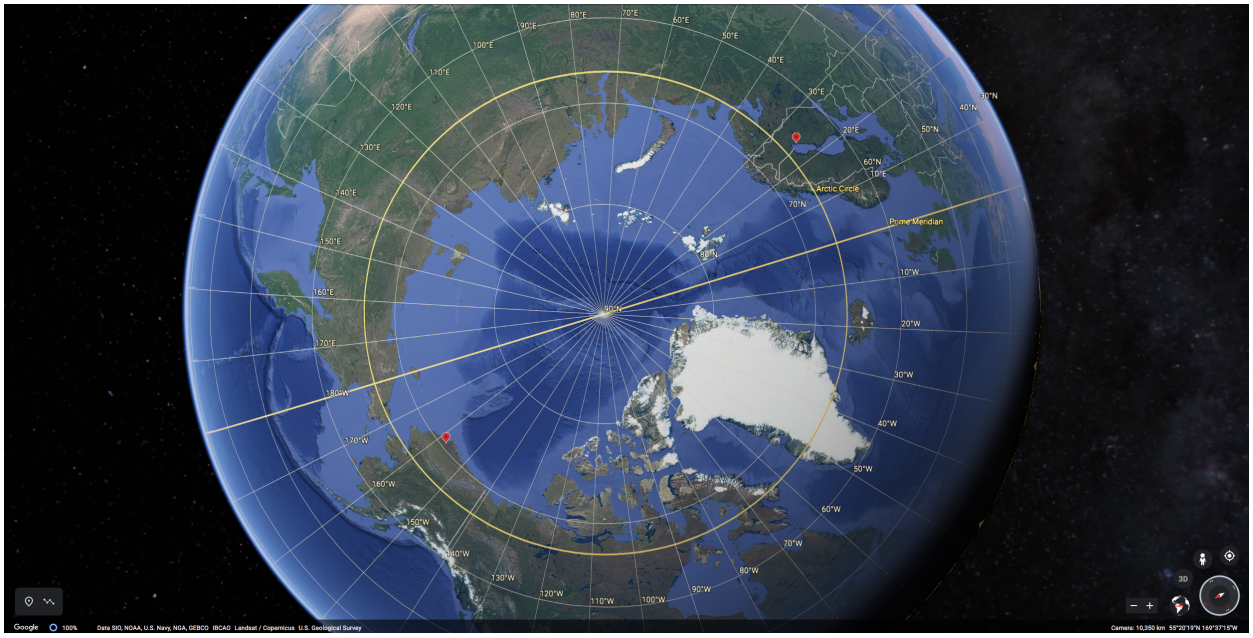

FIG. 1. Google Earth Image showing the locations (red dots) of Hailuoto, Finland (top right) and Utqiaġvik, Alaska, USA (bottom left) .

Boundary Layer (ISOBAR) field campaign (Kral et al. 2018, 2020, in review) and the American Radiation Movement (ARM) data project (Ackerman and Stokes 2003; Mather and Voyles 2013). The ISOBAR Field Campaign took place on the island of Hailuoto, Finland (Figure 1, top right of globe). This island is 20 km off the coast of the city of Oulu, Finland. Being roughly 173 km from the Arctic Circle, the island only sees 7-10 hours of daylight during the winter and experiences brutal, cold weather. The campaign took place from February 6-26, 2018, during the heart of the polar winter. The project utilized a combination of meteorological towers, lidar, sodar, and Unmanned Aircraft Systems (UAS) or Remotely Piloted Aircraft Systems (RPAS) (Segales et al. 2020). The RPAS, known as the CopterSonde, were developed by the University of Oklahoma's Center for Autonomous Sensing and Sampling (CASS). The design is based on a heavily modified airframe with autopilot built in to the software. With the CopterSonde, one can measure atmospheric state variables such as humidity, temperature, wind, and pressure with research-grade accuracy and precision (Greene et al. 2018, 2019; Barbieri et al. 2019; Segales et al. 2020; Bell et al. 2020). Profiles were taken up to a height of around 300 m.

ARM was established by the U.S. Department of Energy in 1989. As described by ARM's official website (`https://arm.gov/about/history`), the founding goal of ARM as "to advance a robust predictive understanding of Earth's climate and environmental systems and to inform the development of sustainable solutions to the Nation's energy and environmental changes". Among three ground sites and several mobile sites located around the world, there are 25 years of atmospheric observations. One of the three active sites is the North Slope of Alaska (NSA) atmospheric observatory in Utqiaġvik (formerly Barrow), Alaska (Figure 1, bottom left of globe). Founded in 1997, the site makes use of 32 different instruments, including radiosondes (Ackerman and Stokes 2003; Mather and Voyles 2013). For this study, 58 radiosonde profiles were utilized from February 2018.

Shown in Figure 1, relative to Hailuoto, Utqiaġvik is 200 km further north of the Arctic Circle. At the northernmost point in Alaska, the city lies directly along the Arctic Ocean. The climate of Northern Finland is moderated by the Gulf Stream, albeit, to a lesser extent of nearby Sweden and Norway. North Alaska is cooled by the cold waters of the Bering Sea and the Arctic. These slight climatic and geographic variations likely impact the makeup of the boundary layer in the two locations.

In analyzing the data, profiles of atmospheric state variables with respect to height in the wintertime boundary layer in these locations were compared. Using data from ISOBAR's CopterSonde and radiosonde data from the NSA site, I will be analyzing profiles of temperature, potential temperature, relative humidity, and wind speed with respect to height. Although the data for the NSA has measurements in the atmosphere as high as 20,000 m, in order to maintain consistency with the ARM data, only the lowest 300 m were examined.

I will also be analyzing the occurrence of inversion layers in the boundary layer. The Mayfield and Fochesatto (2013) algorithm was recreated so it could be applied to temperature profiles from Alaska and Finland. The key ideas of the algorithm are as following:

1. A line is fitted to the first two points of a profile.
2. A third point is added, with a line now fit between three points.
3. The process is repeated with additional point being an added and a line re-fit to the given points, until the root mean squared error $RMSE > 0.1°C$.
4. Steps 1–3 are repeated, taking the top of the previous profile as the new base zb

An error of 0.1°C was chosen because the ARM temperature data had an error of 0.1°C. Once a line has been fit to the profile, one can determine the presence of inversion and stratified layers. For each layer the base (zb) and the lapse rate (m) were defined. Once a layer was determined, it could be classified as a SBI or an EI. An example profile resulting from this algorithm is shown in Figure 2.

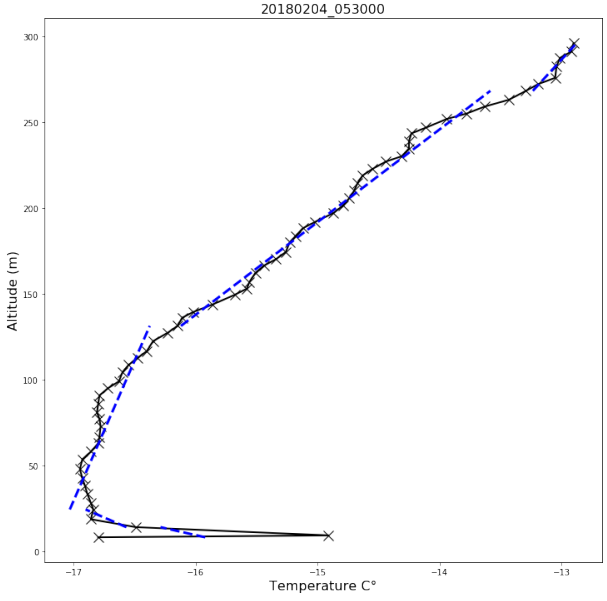

FIG. 2. Example of our algorithm applied to an ARM temperature (°C) profile (The dashed black line is the original profile, while the blue line is the line that was fit to the profile .

3. Results

a. Temperature Environment

Over both sites, inversion and stratified layers were present. However, there was persistent variability in the

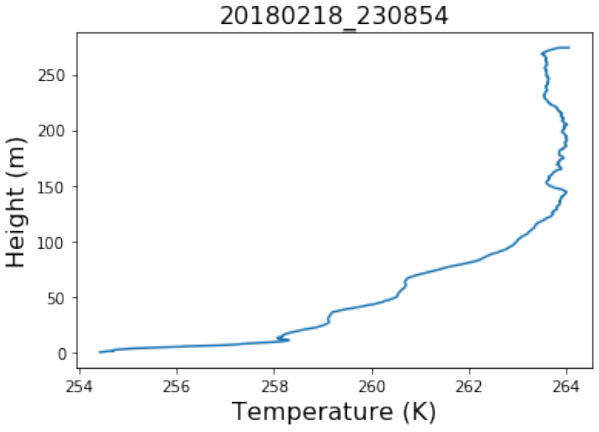

FIG. 3. ISOBAR temperature profile (K) on 18 February 2018 at 23:08:54 UTC.

make-up of these layers over the observed days. Temperature profiles were classified as prominently ground-based inversion, prominently upper-level inversion, positively linear, negatively linear, multi-layered, and inversion/stratified. A plurality of profiles from both sites showed a prominent upper level inversion, 44% over Hailuoto and 25.8% over North Alaska. A prominent ground based inversion occurred at higher frequency, 20.9% over Hailuoto, compared to only 5.2% over North Alaska. In addition, a significant minority of profiles over North Alaska exhibited a nearly linear decrease in temperature with height, 17.2%. Only 7.0% of profiles over Hailuoto showed such decrease. Positively linear profiles were less common, 2.3% over Hailuoto and 8.6% over North Alaska. Profiles where there was neither an upper-level inversion nor a ground based inversion occurred at a greater frequency over North Alaska, 19.0%, compared to Hailuoto, 4.7%. In addition, layers where a ground based inversion transitioned to stratified or isothermal layers were the second most common over Hailuoto and North Alaska, 20.9% and 24.1% respectively. These particular profiles from the 18th and the 20th over Finland show how abruptly the temperature environment can change. Figure 3 shows that on the 18th, temperature steadily increases with height over the first 100 m of the boundary layer. At around 150 m, temperature is roughly constant with height. This indicates an inversion that is largely based in the lower boundary layer. Figure 4 shows that on the 20th, the inversion becomes restricted to the upper levels, with temperature roughly constant from the surface up to nearly 200 m.

Both profiles showed strong lapse rates in potential temperature θ. As with temperature, the magnitude and location of these gradients varied over the observed period. For Hailuoto, the average maximum value of potential temperature was 263.4 K, compared to 248.6 over North Alaska.

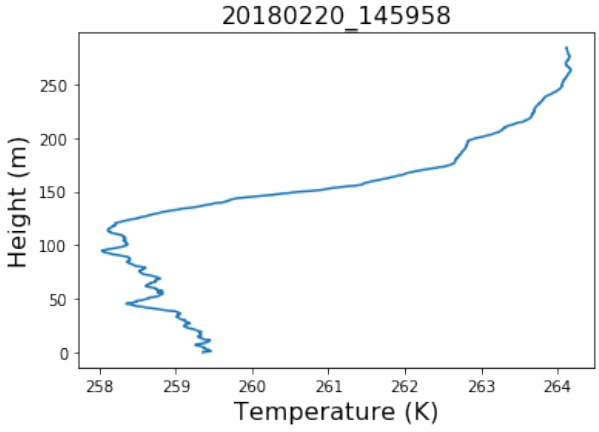

FIG. 4. ISOBAR temperature profile (K) on 20 February 2018 at 14:59:58 UTC. .

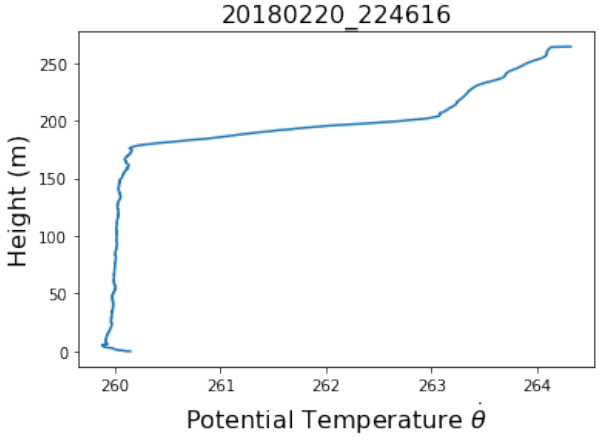

FIG. 5. Potential temperature (K) with height from Hailuoto, Finland on 20 February 2018 at 22:46:16 UTC.

The average height at which the maximum potential temperature occurs 263.9 m over Hailuoto. This height was greater, 282.5 m, over North Alaska. Profiles of potential temperature on the 20th of February from both locations illustrate the different realizations of potential temperature through the boundary layer. In the Figure 5 profile, potential temperature is nearly constant with height in the first 200 m. At around 200 m, potential temperature changes rapidly over the next 50 m. Figure 6 shows potential temperature increasing at a near linear rate over the first 100 m. After 100 m, potential temperature is relatively constant.

b. Wind Environment

The average maximum wind speed over Hailuoto was 3.69 m s^{-1}, occurring at an average height of 227.4 m. The average wind speed over North Alaska was 3.20 m s^{-1}. The average location of the wind max was higher,

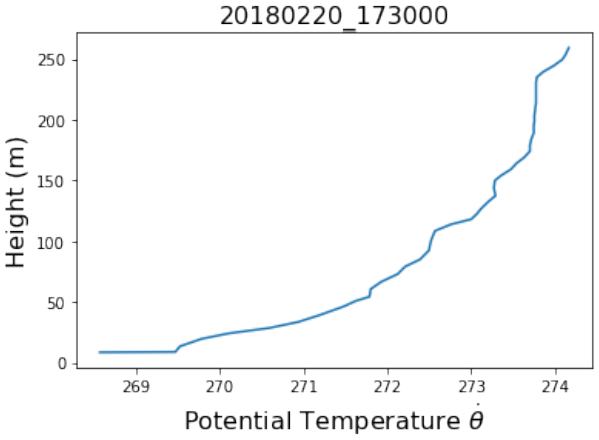

FIG. 6. Potential temperature (K) with height from North Alaska, USA on 20 February 2018 at 17:30:00 UTC. .

at 260.0 m. The higher location of the average wind max over North Alaska indicates a more gradual increase in wind, hence, a less stratified environment. Lower wind gradient corresponds to a less sheared environment. Wind shear can be seen as an indicator of the stability of a profile. Where the atmosphere is stable closer to the surface, wind is suppressed. When the layer above is more buoyant, wind and turbulence become prominent. The difference in wind with height creates a sheared environment. As seen from Figure 7, wind speed over Finland is relatively constant with height until 200 m, where it sharply increases. On the same day in Alaska, Figure 8 shows wind initially decreasing with height, then gradually increasing to reach a maximum at roughly 250 m.

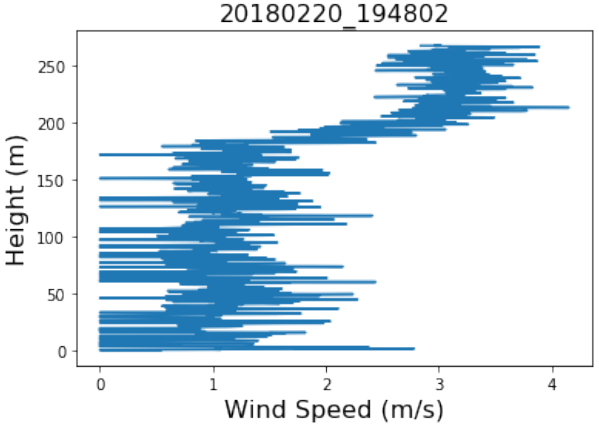

FIG. 7. Unfiltered wind speed (m s^{-1}) with height from Finland on 20 February 2018 at 19:48:02 UTC. .

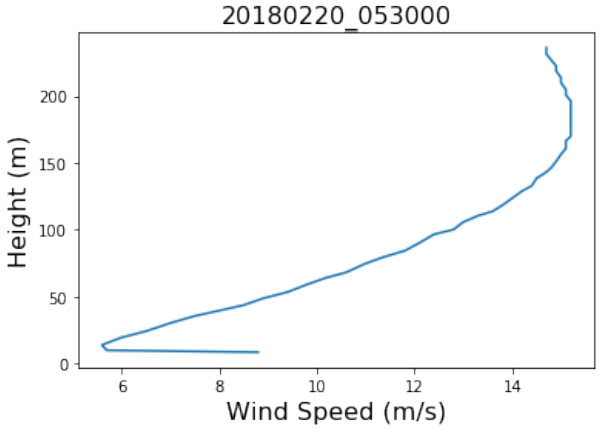

FIG. 8. Wind profile from North Alaska on 20 February 2018 at 05:30:00 UTC. .

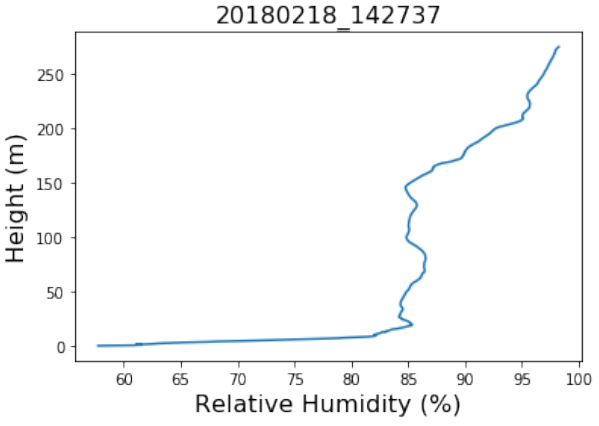

FIG. 10. Profile of relative humidity from Finland on 18 February 2018 at 14:27:37 UTC. .

c. Moisture

A frequent presence of dry-air intrusions were noted over North Alaska. Looking at relative humidity, the lowest recorded value from the radiosonde was 26.3%. The average minimum value was 50%, occurring at 215.7 m. Hailuoto exhibited a less moist environment, with an average minimum value of relative humidity of 81.3% just above the ground. The reason for this disparity is not clear. Although, the dry-air intrusions over North Alaska could be the result of dry-air being advected from the polar ice caps or continental air from Canada and Central Alaska. Looking at the 18th of February, one can see the drier air mass over North Alaska. Figure 9 shows multiple intrusions of dry air at 120 m and 220 m. In Figure 10, values of relative humidity are seen to increase with height, approaching 100% relative humidity at the top of the boundary layer. This potentially signifies clouds at the top of this layer.

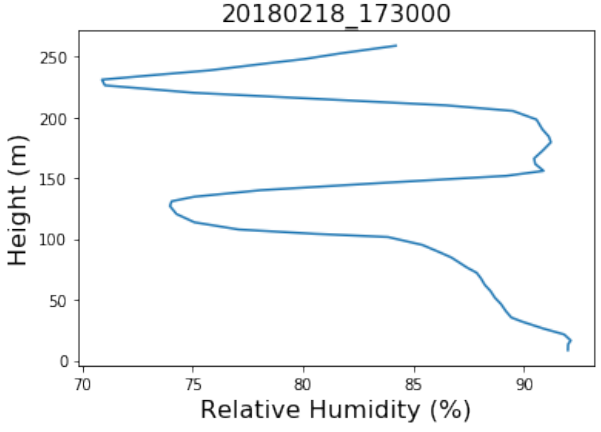

FIG. 9. Profile of relative humidity from North Alaska on 18 February 2018 at 17:30:00 UTC. .

d. Algorithm Results

After applying the Mayfield and Fochesatto (2013) algorithm to profiles from both sites, it was apparent that a layered structure was endemic in the planetary boundary layer (see statistical results in Table d). 100% of profiles had at least one inversion/stratified layer. The total number of layers occurring over Hailuoto was 10. North Alaska showed slightly more, with 11 layers. For the two sites, the average height of the first layer was 40 m. The average height of subsequent layers was approximately 20 m over Hailuoto and approximately 23 m over North Alaska. Interestingly, the average base of the seventh layer over Hailuoto was lower than the average base of the sixth layer. The most likely reason is that, when a seventh layer was present, the base of the sixth layer was significantly lower than average.

The average slope of the first layer was roughly 10 K (100 m)$^{-1}$. For perspective, the dry adiabatic lapse rate is -9.8 K km^{-1}. This means that the average lapse rate over the two locations was not only positive, but about ten times stronger than the dry adiabatic lapse rate. This signifies that an impressively stable inversion layer was present over Finland and North Alaska. The resolution of the lapse rate over the subsequent layers varied over both places. Over North Alaska, the lapse rate was roughly constant with height, hovering between 4 and 5 K (100 m)$^{-1}$. A notable exception to this trend was the ninth layer, where the lapse rate reached a staggering high of 28.3 K (100 m)$^{-1}$. However, in the tenth layer, the lapse rate decreased back to around 4 K (100 m)$^{-1}$. Lapse rates over Finland not only showed greater variance, they also decreased with height. Meaning, the top of the boundary layer over North Alaska was less stable than at the surface.

TABLE 1. Resulting statistics from the modified Mayfield and Fochesatto (2013) algorithm utilized in this study.

	zb (m)		**Lapse rate (K/100 m)**	
	ISOBAR	ARM	ISOBAR	ARM
Layer				
1	0.00	0.00	10.67	8.54
2	39.18	37.9	16.51	4.21
3	75.22	80.08	6.99	4.76
4	92.43	135.25	5.19	4.11
5	120.04	167.28	2.40	4.44
6	146.87	195.15	3.46	5.13
7	143.31	212.34	0.93	4.56
8	176.45	226.84	1.97	3.09
9	195.08	231.69	0.96	28.3
10	230.64	256.00	0.19	3.39
11	265.37		0.5	

4. Conclusions

The boundary layer can be defined by stable or unstable conditions, with stable conditions marked by strong temperature inversions. Additionally, the stable boundary layer is often made up of several layers of inversions. Although the boundary layer is where we live, it is vastly under-sampled and our understanding of the physics, particularly that of the stable boundary layer, are poor. Looking at data from the ISOBAR Field Campaign and the ARM North Alaska site, I aimed to gather a better picture of the stable boundary layer over the Arctic. I found that, like in the Mayfield and Fochesatto (2013) study over Fairbanks, Alaska, the boundary layer over both sites showed a layered structure. The height of the maximum potential temperature and the wind maximum was lower over Hailuoto, signifying a more sheared-and therefore more stable-environment was present there. Over North Alaska, frequent intrusions of dry air were noted, likely due to the advection of continental air from interior Alaska and Canada and dry air from the arctic sea ice. Looking at the layers found, there were slightly more inversion layers over Hailuoto. The average height of each elevated layer was roughly the same. However, the lapse rate remained roughly constant over the elevated layers over North Alaska. It is clear to see that the arctic boundary layer is fluid, varying with location. More locations need to be sampled, and over longer time frames for a better understanding of the stable boundary layer. UAS/RPAS, such as the CopterSonde used in the ISOBAR campaign, have a tremendous potential to further deepen our insights into the small scale structures of the boundary layer.

Acknowledgments. The authors of this paper are honored to thank Daphne LaDue, Alex Marmo, and the Research Experiences for Undergraduates (REU) for their hard work and determination in the face of the Coronavirus Pandemic to make this research possible. I would personally like to thank CASS for all of their work and support in paving the way for this research to be done.

This research has been supported by the National Science Foundation under Grant No. AGS-1560419.

The statements, findings, and conclusions are those of the authors and do not necessarily reflect the views of the National Science Foundation.

References

Ackerman, T., and G. Stokes, 2003: The atmospheric radiation measurement program (vol 56, pg 38, 2003). *PHYSICS TODAY*, **56 (2)**, 14–14.

Andreas, E. L., T. W. Horst, A. A. Grachev, P. O. G. Persson, C. W. Fairall, P. S. Guest, and R. E. Jordan, 2010: Parametrizing turbulent exchange over summer sea ice and the marginal ice zone. *Quarterly Journal of the Royal Meteorological Society*, **136 (649)**, 927–943, doi:10.1002/qj.618.

Barbieri, L., and Coauthors, 2019: Intercomparison of Small Unmanned Aircraft System (sUAS) Measurements for Atmospheric Science during the LAPSE-RATE Campaign. *Sensors*, **19 (9)**, 2179, doi:10.3390/s19092179.

Beare, R. J., and Coauthors, 2006: An Intercomparison of Large-Eddy Simulations of the Stable Boundary Layer. *Boundary-Layer Meteorology*, **118 (2)**, 247–272, doi:10.1007/s10546-004-2820-6.

Bell, T. M., B. R. Greene, P. M. Klein, M. Carney, and P. B. Chilson, 2020: Confronting the boundary layer data gap: Evaluating new and existing methodologies of probing the lower atmosphere. *Atmospheric Measurement Techniques*, **13 (7)**, 3855–3872, doi:10.5194/amt-13-3855-2020.

Couvreux, F., and Coauthors, 2020: Intercomparison of Large-Eddy Simulations of the Antarctic Boundary Layer for Very Stable Stratification. *Boundary-Layer Meteorology*, doi:10.1007/s10546-020-00539-4.

Greene, B. R., A. R. Segales, T. M. Bell, E. A. Pillar-Little, and P. B. Chilson, 2019: Environmental and Sensor Integration Influences on Temperature Measurements by Rotary-Wing Unmanned Aircraft Systems. *Sensors*, **19 (6)**, 1470, doi:10.3390/s19061470.

Greene, B. R., A. R. Segales, S. Waugh, S. Duthoit, and P. B. Chilson, 2018: Considerations for temperature sensor placement on rotary-wing unmanned aircraft systems. *Atmospheric Measurement Techniques*, **11 (10)**, 5519–5530, doi:10.5194/amt-11-5519-2018.

Hoff, R., and R. Hardesty, 2012: Thermodynamic Profiling Technologies Workshop Report to the National Science Foundation and the National Weather Service. Tech. rep., National Center for Atmospheric Research.

Holtslag, A. A. M., and Coauthors, 2013: Stable Atmospheric Boundary Layers and Diurnal Cycles: Challenges for Weather and Climate Models. *Bulletin of the American Meteorological Society*, **94 (11)**, 1691–1706, doi:10.1175/BAMS-D-11-00187.1, URL https://doi.org/10.1175/BAMS-D-11-00187.1, https://journals.ametsoc.org/bams/article-pdf/94/11/1691/3740326/bams-d-11-00187_1.pdf.

Kaiser, A., D. Faranda, S. Krumscheid, D. Belušić, and N. Vercauteren, 2020: Detecting Regime Transitions of the Nocturnal and Polar Near-Surface Temperature Inversion. *Journal of the Atmospheric Sciences*, **77 (8)**, 2921–2940, doi:10.1175/JAS-D-19-0287.1, URL https://doi.org/10.1175/JAS-D-19-0287.1, https://journals.ametsoc.org/jas/article-pdf/77/8/2921/4985822/jasd190287.pdf.

Kral, S., and Coauthors, 2020, in review: The innovative strategies for observations in the arctic atmospheric boundary layer project (ISOBAR). *Bull. Amer. Meteor. Soc.*

Kral, S. T., and Coauthors, 2018: Innovative Strategies for Observations in the Arctic Atmospheric Boundary Layer (ISOBAR)—The Hailuoto 2017 Campaign. *Atmosphere*, **9 (7)**, 268, doi:10.3390/atmos9070268.

Mather, J. H., and J. W. Voyles, 2013: The arm climate research facility: A review of structure and capabilities. *Bulletin of the American Meteorological Society*, **94 (3)**, 377–392.

Mauritsen, T., and G. Svensson, 2007: Observations of Stably Stratified Shear-Driven Atmospheric Turbulence at Low and High Richardson Numbers. *Journal of the Atmospheric Sciences*, **64 (2)**, 645–655, doi:10.1175/JAS3856.1, URL https://doi.org/10.1175/JAS3856.1, https://journals.ametsoc.org/jas/article-pdf/64/2/645/3495663/jas3856_1.pdf.

Mayfield, J. A., and G. J. Fochesatto, 2013: The layered structure of the wintertime atmospheric boundary layer in the interior of alaska. *Amer. Meteor. Soc.*, **52**, 953–957, doi:10.1175/JAMC-D-12-01.1.

National Academies of Sciences, E., 2018a: *The Future of Atmospheric Boundary Layer Observing, Understanding, and Modeling: Proceedings of a Workshop*. doi:10.17226/25138.

National Academies of Sciences, E., 2018b: *Thriving on Our Changing Planet: A Decadal Strategy for Earth Observation from Space*. doi:10.17226/24938.

National Research Council, 2007: *Earth Science and Applications from Space: National Imperatives for the Next Decade and Beyond*. National Academies Press.

Sandu, I., A. Beljaars, P. Bechtold, T. Mauritsen, and G. Balsamo, 2013: Why is it so difficult to represent stably stratified conditions in numerical weather prediction (NWP) models? *Journal of Advances in Modeling Earth Systems*, **5 (2)**, 117–133, doi:10.1002/jame.20013.

Segales, A. R., B. R. Greene, T. M. Bell, W. Doyle, J. J. Martin, E. A. Pillar-Little, and P. B. Chilson, 2020: The CopterSonde: An insight into the development of a smart unmanned aircraft system for atmospheric boundary layer research. *Atmospheric Measurement Techniques*, **13 (5)**, 2833–2848, doi:10.5194/amt-13-2833-2020.

Steeneveld, G., T. Mauritsen, E. De Bruijn, J. Vilà-Guerau de Arellano, G. Svensson, and A. Holtslag, 2008: Evaluation of limited-area models for the representation of the diurnal cycle and contrasting nights in cases-99. *Journal of Applied Meteorology and Climatology*, **47 (3)**, 869–887.

Stull, R. B., 2012: *An introduction to boundary layer meteorology*, Vol. 13. Springer Science & Business Media.

Sullivan, P. P., J. C. Weil, E. G. Patton, H. J. J. Jonker, and D. V. Mironov, 2016: Turbulent Winds and Temperature Fronts in Large-Eddy Simulations of the Stable Atmospheric Boundary Layer. *Journal of the Atmospheric Sciences*, **73 (4)**, 1815–1840, doi:10.1175/JAS-D-15-0339.1.

Sun, J., and Coauthors, 2015: Review of wave-turbulence interactions in the stable atmospheric boundary layer. *Reviews of Geophysics*, **53 (3)**, 956–993, doi:10.1002/2015RG000487.